


# Effects of oxygen concentration and irradiation defects on the oxidation corrosion of body-centered-cubic iron surfaces: A first-principles study

Zhiqiang Ye(叶志强), Yawei Lei(雷亚威), Jingdan Zhang(张静丹), Yange Zhang(张艳革), Xiangyan Li(李祥艳), Yichun Xu(许依春), Xuebang Wu(吴学邦), C. S. Liu(刘长松), Ting Hao(郝汀), and Zhiguang Wang(王志光)

**Citation:**Chin. Phys. B, 2022, 31 (**8**): 086802. DOI: 10.1088/1674-1056/ac633c
Journal homepage: http://cpb.iphy.ac.cn; http://iopscience.iop.org/cpb

**What follows is a list of articles you may be interested in**

---

## First-principles study of high performance lithium/sodium storage of $Ti_3C_2T_2$ nanosheets as electrode materials

Li-Na Bai(白丽娜), Ling-Ying Kong(孔令莹), Jing Wen(温静), Ning Ma(马宁), Hong Gao(高红), Xi-Tian Zhang(张喜田)

Chin. Phys. B, 2020, 29 (**1**): 016802. DOI: 10.1088/1674-1056/ab592e

## Sodium decorated net-Y nanosheet for hydrogen storage and adsorption mechanism: A first-principles study

Yunlei Wang(王云蕾), Yuhong Chen(陈玉红), Yunhui Wang(王允辉)

Chin. Phys. B, 2020, 29 (**1**): 016801. DOI: 10.1088/1674-1056/ab5785

## First-principles study of He trapping in $\eta$-$Fe_2C$

Bing-Ling He(赫丙玲), Jin-Long Wang(王金龙), Zhi-Xue Tian(田之雪), Li-Juan Jiang(蒋利娟), Wei Song(宋薇), Bin Wang(王斌)

Chin. Phys. B, 2016, 25 (**11**): 116801. DOI: 10.1088/1674-1056/25/11/116801

## Interface effect on structural and electronic properties of graphdiyne adsorbed on $SiO_2$ and h-BN substrates: A first-principles study

Dong Bao-Juan, Yang Teng, Wang Ji-Zhang, Zhang Zhi-Dong

Chin. Phys. B, 2015, 24 (**9**): 096806. DOI: 10.1088/1674-1056/24/9/096806

## Corrosion related properties of iron (100) surface in liquid lead and bismuth environments： A first-principles study

Song Chi, Li Dong-Dong, Xu Yi-Chun, Pan Bi-Cai, Liu Chang-Song, Wang Zhi-Guang

Chin. Phys. B, 2014, 23 (**5**): 056801. DOI: 10.1088/1674-1056/23/5/056801

---

# Effects of oxygen concentration and irradiation defects on the oxidation corrosion of body-centered-cubic iron surfaces: A first-principles study

Zhiqiang Ye(叶志强)[1,2], Yawei Lei(雷亚威)[1,2], Jingdan Zhang(张静丹)[1,2], Yange Zhang(张艳革)[1,2,†], Xiangyan Li(李祥艳)[1,2], Yichun Xu(许依春)[1,2,‡], Xuebang Wu(吴学邦)[1,2], C. S. Liu(刘长松)[1,2], Ting Hao(郝汀)[3], and Zhiguang Wang(王志光)[4]

[1] *Key Laboratory of Materials Physics, Institute of Solid State Physics, HFIPS, Chinese Academy of Sciences, Hefei* 230031, *China*
[2] *University of Science and Technology of China, Hefei* 230026, *China*
[3] *School of Mechanical Engineering, Suzhou University of Science and Technology, Suzhou* 215009, *China*
[4] *Institute of Modern physics, Chinese Academy of Sciences, Lanzhou* 730000, *China*

(Received 27 December 2021; revised manuscript received 15 March 2022; accepted manuscript online 1 April 2022)

Oxidation corrosion of steels usually occurs in contact with the oxygen-contained environment, which is accelerated by high oxygen concentration and irradiation. The oxidation mechanism of steels is investigated by the adsorption/solution of oxygen atoms on/under body-centered-cubic (bcc) iron surfaces, and diffusion of oxygen atoms on the surface and in the near-surface region. Energetic results indicate that oxygen atoms prefer to adsorb at hollow and long-bridge positions on the Fe(100) and (110) surfaces, respectively. As the coverage of oxygen atoms increases, oxygen atoms would repel each other and gradually dissolve in the near-surface and bulk region. As vacancies exist, oxygen atoms are attracted by vacancies, especially in the near-surface and bulk region. Dynamic results indicate that the diffusion of O atoms on surfaces is easier than that into near-surface, which is affected by oxygen coverage and vacancies. Moreover, the effects of oxygen concentration and irradiation on oxygen density in the near-surface and bulk region are estimated by the McLean's model with a simple hypothesis.

**Keywords:** oxidation corrosion, oxygen concentration, irradiation defects, bcc-Fe surfaces, first-principles study

**PACS:** 68.43.Bc, 73.20.Hb, 28.52.Fa **DOI:** 10.1088/1674-1056/ac633c

## 1. Introduction

Oxidation corrosion is an important problem for steels operating in oxygen-contained environments. It becomes severe when the steels as structural materials are in contact with coolant with high oxygen concentration and irradiation environments in nuclear reactors. The severe corrosion can lead to rapid growth in the oxidation layer on the surface of structural materials. The increased oxidation layer not only significantly reduces the heat conduction of structural materials but also increases the lockage risk of the coolant loop due to the spalling of oxidation. Therefore, it is necessary to understand how the oxidation layer is formed and which factors affect the growth of the oxidation layer on the iron (Fe)-based structural materials.

The oxidation layer on the Fe-based structural materials is usually composed of the outer oxide layer ($Fe_3O_4$) and the inner oxide layer ($(Fe, Cr)_3O_4$),[1,2] as in contact with the oxygen-contained environment from experimental research. An available space model was proposed to explain the formation mechanism of the oxide layer on the surface of Fe-based structural materials in oxygen-contained environments.[1,2] In this model, Fe atoms go out and combine with oxygen atoms outside forming the outer oxidation layer, $Fe_3O_4$, meanwhile, leaving enough space for oxygen atoms coming into the bulk-forming inner oxidation layer $(Fe, Cr)_3O_4$. The growth rate of the oxidation layer depends on the migration rate of cations in the oxidation layer and the oxygen concentration at the interface,[3] which depends on temperature,[4–6] oxygen concentration[4,5,7,8] and irradiation dose.[9,10] Yeliseyeva[4] revealed that the corrosion rates for T91 and AISI 316L steels increase with increasing temperature. Gorynin[7] found that the concentration of oxygen in liquid metals (lead or lead-bismuth eutectic, LBE) determines the corrosion of steels. High oxygen concentration ($> 10^{-6}$%) leads to oxidation corrosion, which is accelerated rapidly with increasing oxygen concentration, although low oxygen concentration ($10^{-10}$%–$10^{-8}$%) results in dissolution corrosion. Frazer[9] found that passive oxide structures grow on the ferritic/martensitic steel HT9 in contact with oxygen-contained LBE while being irradiated, even the oxidation layer is greatly increased by the irradiation and spall off the surface. Meanwhile, irradiation not only affects the thickness of the oxidation layer but also changes the structure of the oxidation layer.[10] However, the micro-pictures of oxygen atoms adsorbing on the surfaces and

†Corresponding author. E-mail: yangezhang@issp.ac.cn
‡Corresponding author. E-mail: xuyichun@issp.ac.cn

© 2022 Chinese Physical Society and IOP Publishing Ltd 

migrating into the bulk in high oxygen concentration and irradiation environments cannot be observed by these experiments at the initial oxidation stage.

Some theoretical simulations have been investigated to explore the formation of oxidation,[11–17] such as adsorption properties of oxygen on the body-centered-cubic (bcc)-Fe surfaces and the solution and diffusion of oxygen in bcc-Fe bulk. Based on density functional theory, people found that oxygen molecules ($O^2$) dissociate firstly, then energetically adsorb at the hollow position on the Fe(100) and long-bridge position on Fe(110) surface. The adsorption depends on the coverage of oxygen atoms and alloying atoms on the surfaces.[14,18,19] In the bulk, oxygen atoms prefer to solute at octahedral interstitial sites (OCT) of the Fe lattice[15,16] and diffuse quickly to the next OCT site with the energy barrier of 0.54 eV.[17] However, they are easily trapped by vacancy defects and grain boundaries, which also slow down the diffusion of oxygen.[20–22] Besides, the effects of alloying atoms on the solution and diffusion of oxygen are also explored in Fe-based alloys.[21,23] The bond order analysis potential of the Fe–O system has been proposed to reproduce the fundamental properties of the Wustite and the energetics of oxygen atoms in $\alpha$-iron.[24] However, little literature has clarified the micro-picture of the oxidation process at the initial stage: how oxygen atoms migrate and dissolve in the near-surface region after adsorption on the surfaces, and how the oxygen concentration and irradiation affect the solution and migration of oxygen atoms?

In this paper, we aim to acquire the mechanism of oxidation corrosion by focusing on the adsorption/solution properties of oxygen atoms on/under the Fe(100) and Fe(110) surfaces as well as their dependences on oxygen coverage and irradiation defects, and the migration properties of oxygen atoms. Firstly, the basic properties of clean surfaces, such as their surface energies, electronic work function and magnetic moments are investigated by the first-principles calculations to make sure the reasonable models and parameters are used in this work. Then, the adsorption properties of oxygen atoms on Fe surfaces are explored by the adsorption energies of O atoms at the most stable positions on Fe(100) and Fe(110) surfaces with different coverage. The insight into the local structure is explored by the charge density difference and the electronic local density of states at the atomic level. In addition, the influence of oxygen concentration and vacancy defects on the solution and migration of oxygen atoms are studied to derive the micro-picture of oxidation corrosion of Fe surfaces. Finally, the effects of oxygen concentration and vacancy on the oxidation corrosion of Fe surfaces are further discussed in contact with oxygen-contained environment and irradiation.

## 2. Model and method

### 2.1. Computational details

All calculations presented here have been performed using the density functional theory (DFT) implemented in the Vienna *ab-initio* simulation package (VASP).[25,26] The generalized gradient approximation (GGA) with the exchange–correlation energy of Perdew–Burke–Ernzerhof (PBE) is adopted.[27] The interaction between ions and electrons is represented by the projector augmented wave (PAW) potentials method with the $3d^7 4s^1$ electrons treated as valence electrons for Fe atoms.[28–30] As a result of the convergence tests, the cutoff energy of 500 eV is used to expand the electronic wave functions, and the first order Methfessel–Paxton method with the Fermi surface smearing of 0.20 eV is adopted to accelerate the convergence. The spin polarization of Fe is performed because of its magnetic properties. With the *k*-point mesh of $12\times12\times12$, the lattice constant of the body-centered-cubic iron (bcc-Fe) is optimized to be 2.831 Å, which is consistent with experimental data and other DFT calculations.[31–33]

The two clean surfaces of bcc-Fe with low index (100) and (110) are modeled by the optimized unit lattice with a 15 Å vacuum layer between the periodic slabs in [001] and [110] directions, respectively. As shown in Fig. 1, the Fe(100) and Fe(110) surfaces consist of a $3\times3$ unit cell with 9 atomic layers. A *k*-point mesh of $5\times5\times1$ is generated automatically using the Monkhorst–Pack method.[34] The bottom three layers in dashed squares are fixed as bulk in Figs. 1(a) and 1(b), and the rest layers are fully relaxed to mimic Fe(100) and Fe(110) surfaces until the force convergence of 0.01 eV/Å.

The O atoms adsorbed surfaces are constructed based on the optimized clean surfaces with oxygen atoms at different high-symmetric sites to determine the lowest energy configuration. As labeled in Fig. 1, hollow (H), bridge (B) and top (T) positions are considered on the Fe(100) surface, and long-bridge (LB), short-bridge (SB) and top (T) sites are considered on the Fe(110) surface. The configuration with the lowest energy is chosen as the most stable one and then utilized to analyze the adsorption/solution properties of oxygen atoms on/under the two surfaces. For investigating the coverage ($\theta$) dependence of the adsorption/solution properties, the stable configurations are initiated by adding a different number of adatoms on the surfaces, corresponding $\theta$ from 0 to 1. For example, one adatom and nine adatoms on the $3\times3$ unit cell (surface atoms as shown in Fig. 1) correspond to the monolayer coverage of 1/9 and 1, respectively. The *k*-points and cutoff energy are tested until the deviation of total energies for the systems is within 0.05 eV.

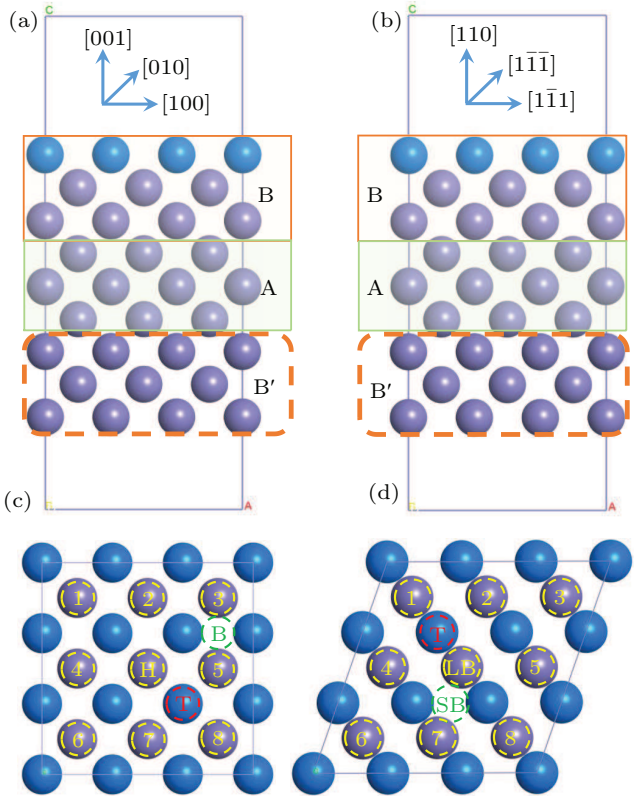



**Fig. 1.** The side view of Fe(100) surface (a), and Fe(110) surface (b), and the overview of Fe(100) (c) and Fe(110) (d), respectively. Orange dashed squares labeled B represent relaxed surface, while labeled B′ represent bottom surface with fixed layers, and the middle cyan region labeled A is the bulk-like region. The blue balls are surface Fe atoms, and the gray balls are Fe atoms at sub-layers. Yellow dashed circles represent the high-symmetric positions for adatoms on a different surface, such as hollow (H), bridge (B) and top (T) on the (100) surface, and long-bridge (LB) and short-bride (SB) on the (110) surface. The numbers 1, 2, 3, …, 8 represent other H positions on the (100) surface, LB on the (110) surface.

### 2.2. Analysis technology

The surface energy of the model with different atomic layers is firstly investigated to avoid the periodic effect of the surface for assuring the reliability of the model. The surface energy $E_s$ is defined as[35–39]

$$E_s = (E_{slab} - nE_{bulk})/2A, \tag{1}$$

where $E_{slab}$ is the total energy of the clean surface slab, $n$ and $E_{bulk}$ are the number of Fe atoms and the energy of each Fe atom in bulk. Meanwhile, the relaxation of the distance $d_{ij}$ between two subsequent $i$, $j$ layers is defined as the following equation to double-check the structure properties:[12,38,40]

$$\Delta_{ij}=(d_{ij}-d)/d, \tag{2}$$

where $d$ is an interplanar spacing in the bulk. The positive sign $\Delta_{ij}$ means expansion, while a negative value means contraction.

Oxygen atoms have to be adsorbed on the Fe surfaces and penetrate the bulk, as oxidation happens. To characterize the capability of oxygen atoms adsorbing/solving on/under the surfaces, we define the adsorption energies/solution energies of oxygen atoms on/under the surfaces as the following equation:[41–49]

$$E^{nO}_{ads/sol} = E^{nO}_{slab} - E_{slab} - \frac{n}{2}E^{O_2}, \tag{3}$$

where $E^{nO}_{ads}$ and $E_{slab}$ are the total energies of the slab with and without $n$ adatoms, respectively. $E^{O_2}$ is the energy of an $O_2$ molecule in the gas phase. According to the definition, a negative $E^{nO}_{ads}$ represents that the adsorption of oxygen atoms is exothermic and occurs spontaneously, while a positive value indicates an endothermic process.

To describe the interactions between oxygen atoms, the binding energy of $n$ oxygen atoms $E^{nO}_{bin}$ is defined as[50]

$$E^{nO}_{bin} = E^{(n-1)O}_{slab} + E^{O}_{slab} - (E^{nO}_{slab} + E_{slab}), \tag{4}$$

where $E^{(n-1)O}_{slab}$, $E^{nO}_{slab}$ and $E^{O}_{slab}$ are the total energy of slab with $(n-1)$, $n$ and one oxygen atom, respectively. Similarly, the interaction between vacancy (v) and O atoms is described by the binding energy $E^{v+O}_{bin}$,

$$E^{v+O}_{bin} = E^{v}_{slab} + E^{O}_{slab} - (E^{v+O}_{slab} + E_{slab}), \tag{5}$$

where $E^{v+O}_{slab}$ is the total energies of the slab with a vacancy and an adsorbing O atom and $E^{v}_{slab}$ is the total energies of the slab with a vacancy. According to the definition, a positive $E^{nO}_{bin}/E^{v+O}_{bin}$ represents the attraction between O atoms or between vacancy and O atom, while a negative value indicates rejections between them.

## 3. Results and discussion

### 3.1. Basic properties of clean Fe(100) and (110) surfaces

The surface energies of the models with different layers and unit cells are firstly explored and shown in Table 1 to check the reliability of models. The surface energy is almost constant as the model expands in surface and layer, indicating that a surface model of $3\times3$ supercell and 9 atomic layers is sufficient and economic in the study. According to Eq. (1), the surface energies calculated for Fe(100) and Fe(110) surfaces are 2.49 J/m$^2$ and 2.41 J/m$^2$, respectively. Those results are in very good agreement with experimental data and other theoretical results, such as 2.48 J/m$^2$ [39,51] of Fe(100), 2.43 J/m$^2$ [38,51] of Fe(110). The work function defined as the difference between the electrostatic potential energy in vacuum zone and the Fermi level are calculated to be 3.86 eV for Fe(100) surface and 4.75 eV for Fe(110) surface, respectively, which show a good agreement with previous results (3.90 eV[12,51] for Fe(100), 4.77 eV[12,38,51,52] for Fe(110)). The magnetic moments of Fe atoms on Fe(100) and Fe(110) surfaces are 2.96 $\mu_B$ and 2.60 $\mu_B$, which are also consistent with our previous results (2.95 $\mu_B$ [18,39,42,51] for Fe(100), 2.59 $\mu_B$ [12,38,51] for Fe(110)). These results indicate that our models are reasonable and calculations are credible.

**Table 1.** Convergence of surface energy $E_s$ and magnetic moments of Fe atoms for Fe(100) and Fe(110) surface.

| Surface cell | $E_s$ (eV) | Mag. ($\mu_B$) |
|---|---|---|
| $3\times3\times5$ (100) | 2.44 | 2.96 |
| $3\times3\times7$ (100) | 2.46 | 2.96 |
| $3\times3\times9$ (100) | 2.49 | 2.96 |
| $3\times3\times11$ (100) | 2.49 | 2.96 |
| $4\times4\times9$ (100) | 2.48 | 2.96 |
| $3\times3\times5$ (110) | 2.43 | 2.59 |
| $3\times3\times7$ (110) | 2.42 | 2.59 |
| $3\times3\times9$ (110) | 2.41 | 2.59 |
| $3\times2\times9$ (110) | 2.41 | 2.60 |
| $3\times2\times11$ (110) | 2.41 | 2.57 |

Figure 2 shows the relaxation of the interplanar distance of Fe(100) and Fe(110) surfaces with and without fixed atoms on the bottom three layers according to Eq. (2). In the models of Fe(100) and (110) surfaces, the interplanar distances $d_{45}$ and $d_{56}$ in zone-A tend to be 0, which indicates that zone-A is the bulk-like region in the model. The $d_{12}$, $d_{23}$ and $d_{34}$ in the near up-surface region (zone-B) show similar behavior for the surfaces with and without fixed atoms on the bottom three layers, although $d_{67}$, $d_{78}$ and $d_{89}$ for the near down-surfaces show the visible difference. These results indicate that the surface models with fixed bottom three layers can be economically used in the following studies to investigate the interactions between oxygen atoms and surfaces. On the Fe(100) surface, the interplanar distance $d_{12}$ decrease by 1.73%, while $d_{23}$ and $d_{34}$ increase by 3.46% and 0.78% respectively, compared with the bulk. On the Fe(110) surface, $d_{12}$ and $d_{23}$ expand by 0.16% and 0.83%, respectively. They are in good agreement with other calculations and experimental results.[12,38,51,53]

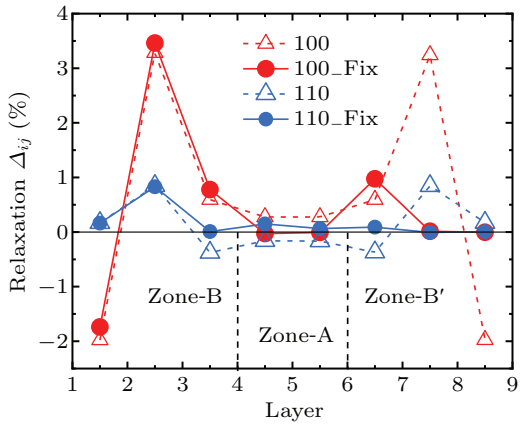



**Fig. 2.** The relaxation of the interplanar distance for the clean Fe (100) and (110) surfaces. The red and blue solid circles show the relaxation of the interplanar distance for the surfaces with fixed bottom three layers, while the red and blue hollow triangles indicate the relaxation of the interplanar distance for the fully relaxed surfaces. The black solid lines show the relaxation of the layer spacing relative to the bulk. Zone-A, zone-B and zone-B′ represent bulk-like region and surface regions. Respectively, as shown in Figs. 1(a) and 1(b).

### 3.2. Adsorption properties of oxygen atoms on Fe surfaces

The adsorption energies of O atoms at different highly symmetric positions on these two surfaces can be calculated by Eq. (3) to investigate the adsorption properties. The results shown in Table 2 indicate that all the $E_{ads}^{nO}$ are negative and O atoms can be easily adsorbed on the Fe surfaces. Meanwhile, the adsorption energies $E_{ads}^{1O}$ at H position on Fe(100) and LB position on Fe(110) are the lowest, indicating that H and LB positions are the most stable positions for O atoms. Therefore, the O atoms are placed at the H positions on Fe(100) and the LB positions on Fe(110) as a priority in subsequent studies. Furthermore, the $E_{ads}^{1O}$ on the Fe(100) is slightly less than that on Fe(110), which implies that the adsorption of O atoms on Fe(100) has a little priority over on Fe(110) surface.

**Table 2.** Adsorption energy of one O atom ($E_{ads}^{1O}$ in eV) at different high-symmetric sites on the clean Fe(100) and Fe(110) surfaces.

| Position | $E_{ads}^{1O}$ (eV) | Position | $E_{ads}^{1O}$ (eV) |
|---|---|---|---|
| H(100) | –4.03 | LB(110) | –3.98 |
| B(100) | –3.42 | SB(110) | –3.52 |
| T(100) | –2.67 | T(110) | –2.15 |

The surface dependence of the adsorption of O atoms on Fe surfaces is further investigated by the charge density difference at the interface between O atoms and Fe surfaces according to previous investigations.[13,54] The charge density difference ($\Delta\rho$), is defined by the total charge of the slab with an adatom subtracted by the total charge of the slab and the adatom. Negative $\Delta\rho$ represents that local electrons are depleted, and positive $\Delta\rho$ means that local electrons are accumulated. Figure 3 shows the $\Delta\rho$ distributions around O atoms on the Fe(100) and Fe(110) surfaces both in the side and top views, respectively. It is noticed that there are substantial rearrangements of electrons around the adsorbed O atoms and Fe atoms on the two surfaces. The $\Delta\rho$ values around O atoms are positive, indicating the electrons around Fe atoms are transferred to the O atoms on the surface. On the Fe(100) surface, the adsorbed O atoms accumulate more electrons than those on the Fe(110) surface. The charge depletion is also checked based on the Bader's theory.[55,56] Relative to the 6 valence electrons for O atoms ($2s^2p^4$), they accumulate 1.34$e$ and 1.16$e$ within their Bader volume on the Fe(100) and Fe(110) surfaces, respectively. The transferred charges from Fe atoms to O atoms on the surface are greater than 0.83$e$ as in bulk bcc-Fe. These results indicate that the interaction between O and Fe atoms on the Fe(100) surface is stronger than on the Fe(110) surface, and the ionic character of Fe–O interaction on the surfaces is stronger than that in the bulk. The ionic character is further investigated by the density of state analysis of O atoms and their adjacent Fe atoms on the two surfaces as shown in Figs. 3(c) and 3(f). The electronic density of p-state for O atoms exhibits sharp peaks with narrow energy range, indicating that localized character of the electronic density of O-2p orbitals, and O-2p and Fe-3d orbitals show weak hybridization. Meanwhile, the charge transfer of Fe atoms under the Fe(100) is affected by the adsorbed O atoms more severely than that below the Fe(110) surface.

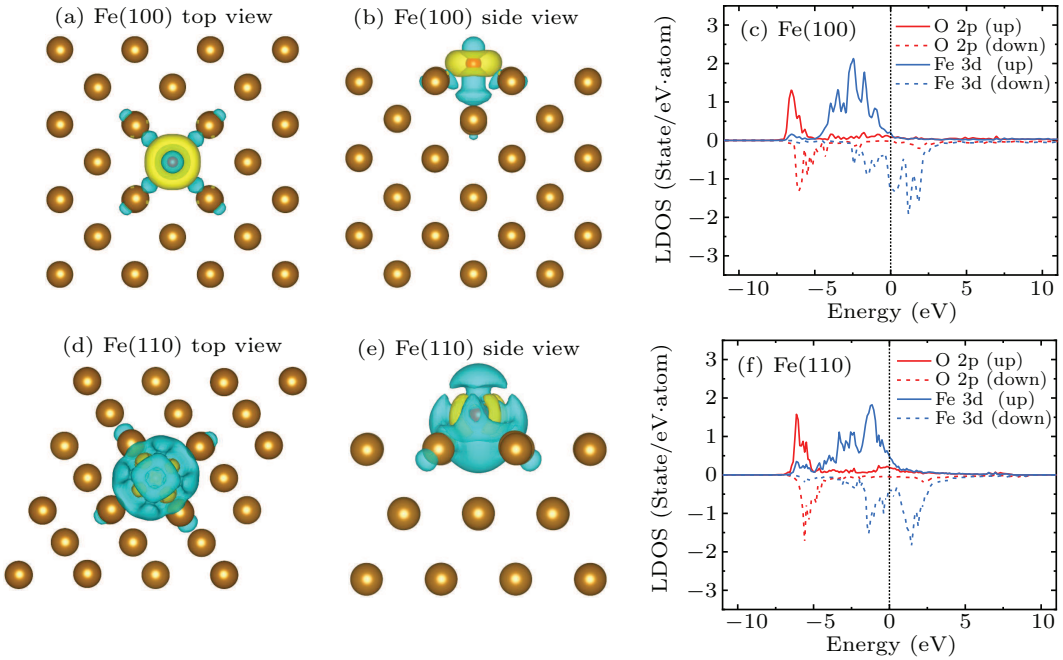



**Fig. 3.** Charge density difference of an O atom at H position on Fe (100) in top view (a) and side view (b), and at LB position on Fe(110) in top view (d), and side view (e) and the electronic local density of states (LDOS) of an O atom at H position on Fe (100) (c) and at LB position on Fe(110) (f). Yellow and blue colors refer to electron accumulation and depletion zones, respectively. Brown and red balls are labeled as Fe and O atoms, respectively. The iso-surface of charge density is 0.008 $e$/Bohr$^3$. Positive/negative values of LDOS represent majority/minority spin states, respectively. The vertical dash line marks Fermi level.

**Table 3.** The lowest adsorption energies of the last O atom ($E_{\rm ads}^{\rm lastO}$) and the n O atoms with the most stable configurations ($E_{\rm ads}^{n\rm O}$) on the Fe(100) and Fe(110) surfaces with different coverage, and the number of O atoms in the first nearest neighbors (1NN) and second nearest neighbors (2NN) on the two surfaces with different.

| $\theta$ | Config. (100) | $E_{\rm ads}$ | 1NN | 2NN | $\theta$ | Config. (110) | $E_{\rm ads}$ | 1NN | 2NN |
|---|---|---|---|---|---|---|---|---|---|
| 0/9 | H | –4.03 | 0 | 0 | 0/9 | LB | –3.96 | 0 | 0 |
| 1/9 | H1 | –3.99 | 0 | 1 | 1/9 | LB3 | –3.90 | 0 | 1 |
| 2/9 | H18 | –3.91 | 0 | 3 | 2/9 | LB36 | –3.72 | 0 | 3 |
| 3/9 | H186 | –3.80 | 2 | 4 | 3/9 | LB362 | –3.10 | 2 | 4 |
| 4/9 | H1862 | –3.78 | 4 | 6 | 4/9 | LB3628 | –3.02 | 4 | 6 |
| 5/9 | H18625 | –3.80 | 6 | 9 | 5/9 | LB36285 | –2.37 | 7 | 8 |
| 6/9 | H186254 | –2.88 | 10 | 11 | 6/9 | LB362851 | –2.21 | 10 | 11 |
| 7/9 | H1862547 | –2.92 | 14 | 14 | 7/9 | LB3628517 | –1.84 | 14 | 14 |
| 8/9 | H18625473 | –3.00 | 18 | 18 | 8/9 | LB36285174 | –1.85 | 18 | 18 |
| 9/9 | H18625473B | –0.62 | – | – | 9/9 | LB3628517T | 1.56 | – | – |

Coverage dependence of oxygen atoms adsorbing on Fe surfaces is further investigated since more and more oxygen atoms would be adsorbed on the Fe surfaces as in contact with oxygen-contained environments. Firstly, the most stable configurations of O atoms with the lowest $E_{\rm ads}^{n\rm O}$ values shown in Table 3 are selected from a large number of calculated $E_{\rm ads}^{n\rm O}$ of O atoms on the Fe surfaces with different configurations and coverages. As shown in Fig. 4, the lowest $E_{\rm ads}^{n\rm O}$ values of $n$ O atoms on the Fe(100) and Fe(110) surfaces generally decrease with the increase in the coverage, indicating that the adsorption of $n$ O atoms occurs automatically. However, the $E_{\rm ads}^{\rm lastO}$ of last one O atom increases, as the coverage of O atoms increases, indicating the repulsion between the adsorbing O atom and pre-adsorbed O atoms. On the Fe(100) surface, the $E_{\rm ads}^{\rm lastO}$ value increases slightly as the coverage increases from 0 to 5/9, then suddenly increases significantly (from $-3.80$ eV to $-2.88$ eV) at coverage of 0.67. When all the hollow positions are occupied by O atoms ($\theta = 1$), an adsorbed O atom has to stay at the bridge position with $E_{\rm ads}^{\rm lastO}$ of $-0.62$ eV, which is greater than the solution energy of an O atom in bulk. On the Fe(110) surface, the $E_{\rm ads}^{n\rm O}$ and $E_{\rm ads}^{\rm lastO}$ show a similar trend as those on the Fe(100) surface, however, the $E_{\rm ads}^{\rm lastO}$ increases quickly even at the low coverage of 0.33, and reaches 1.56 eV at O coverage of 1. This indicates that the coverage dependence of adsorption on the Fe(110) surface is stronger than that on the Fe(100) surface. Meanwhile, the binding energies of the last adsorbed O atom to the other adsorbed O atoms are calculated by Eq. (4) and shown in Fig. 4. They are generally negative, indicating that O atoms repel each other. The $E_{\rm bin}^{n\rm O}$ of two O atoms are very small on both Fe(100) and (110) surfaces, such as $-0.03$ eV on the Fe(100) surface, and $-0.06$ eV on Fe(110) surface, indicating that the weak repulsion between two O atoms on the surfaces with low coverage. However, the $E_{\rm bin}^{n\rm O}$ decrease quickly at high coverage, indicating that

the higher the coverage of O atoms, the severer repulsion between O atoms. Moreover, the repulsion between O atoms on Fe(110) surface is generally greater than that on Fe(100) surface, because Fe(110) surface is closer than Fe(100) surface.

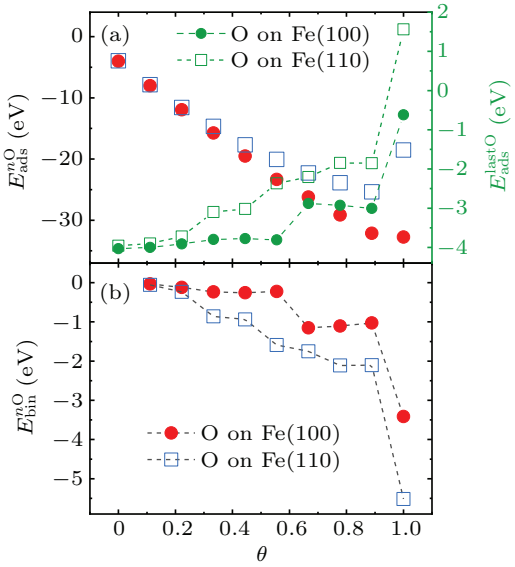



**Fig. 4.** (a) Adsorption energies ($E_{ads}^{nO}$) of O atoms and (b) binding energies ($E_{bin}^{nO}$) of O atoms on the (100) and (110) surfaces with different coverage. The green solid circles and open squares in (a) indicate the adsorption energies ($E_{ads}^{lastO}$) of the last adsorbed O, corresponding to the right scale.

The quick increase in $E_{ads}^{lastO}$ and decrease in $E_{bin}^{nO}$ with the increasing coverage on the two surfaces are further characterized by the change in the positions of Fe atoms on the surfaces and adsorbed O atoms. As shown in Fig. 5(a), when the coverage of O atoms increases, the average positions of O atoms on the Fe(100) surface are almost not changed in the [100] direction until the coverage reaches 1, but on the Fe(110) surface gradually increase in the [110] direction. Meanwhile, the distances of Fe atoms from both surfaces increase, as the coverage of O atoms increase. This indicates that Fe atoms are gradually pulled out by the O atoms on the two surfaces, and O atoms on the Fe(110) surface repel each other more severely than those on the Fe(100) surface. The repulsion depends on the density of O atoms on the surface, which can be seen from the smallest distance between the first nearest neighbor O atoms ($d_{1NNO-O}$). As shown in Fig. 5(b), when the coverage of O atoms increases, the $d_{1NNO-O}$ decreases, therefore, the repulsion between O atoms increases. The higher density of O atoms on the Fe(110) surface leads to the smaller $d_{1NNO-O}$ than that on the Fe(100) surface, so that the repulsion between O atoms on the Fe(110) surface is greater than that on the Fe(100) surface. Especially, as the coverage of O atoms on the Fe(110) surface reaches 1, the $d_{1NNO-O}$ on the Fe(110) surface is about 1.25 Å, and an $O_2$ molecular forms on the surface. This is consistent with the results of energetics results shown in Fig. 4.

The coverage dependences of $E_{ads}^{lastO}$ and $E_{bin}^{nO}$ on the Fe(100) surface are further investigated by charge transfer around the last adsorbed O atom and the number of the first nearest neighbors (1NN) and second nearest neighbors (2NN) around the last adsorbed O atom on the two surfaces. Figure 6 shows the charge density difference around the 7th and 10th atom adsorbed on the Fe(100) surface with coverage of 0.67 and 1.0 inside view and top view. Clearly, the 7th and 10th adsorbed O atoms not only change the charges around neighbor Fe atoms but also interact with pre-covered O atoms, relative to the charge transfer of an O atom at low coverage in Fig. 3. As the coverage of O atoms increases, more charges around Fe atoms on the surfaces ($Fe_1$) are transferred to O atoms, so that the charges between Fe atoms on the surface and subsurface ($Fe_2$) are depleted as shown in Figs. 6(b) and (c). This weakens the bond between $Fe_1$ and $Fe_2$, especially, two $Fe_1$ atoms ($Fe_1^{out}$) are pulled out, when the 10th O atom adsorbs on the bridge position as shown in Figs. 6(c) and 6(f). Meanwhile, the re-arranged charges around pre-covered O atoms indicate the repulsion of the last adsorbed O atom as in Figs. 6(a), 6(d), 6(e) and 6(f). The repulsion interaction between O atoms can also be characterized by the coordination number of its first and second neighbors. When the coordination number of the first nearest neighbor increase (e.g., from 4 to 6/7 on Fe(100)/(110)), $E_{ads}^{lastO}$ increases quickly. As the coordination number of the first nearest neighbor increases, the repulsion between O atoms becomes strong. In a word, with the aggregation of O atoms, the adsorption of O atoms on the surface becomes difficult due to the repulsion between O atoms.

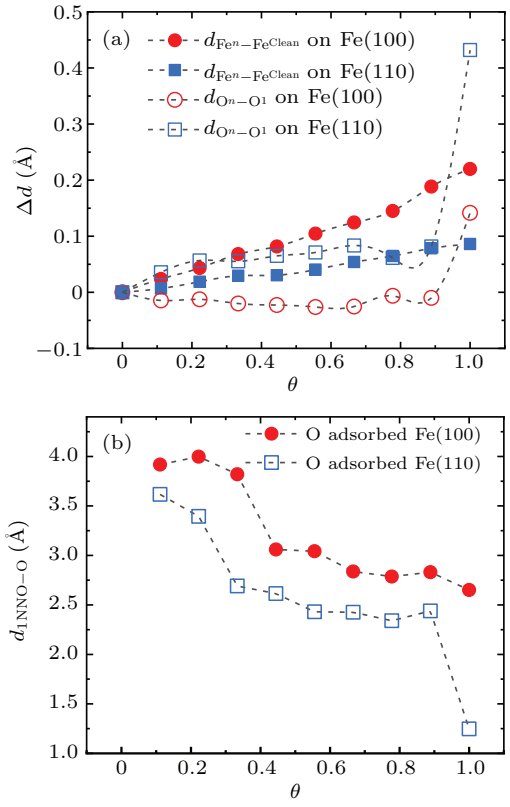



**Fig. 5.** (a) The change in the average positions of Fe atoms and the average distances of O atoms to the first adsorbed O atom on the surfaces as function of the oxygen coverage ($\theta$). (b) The nearest distance between O atoms as function of $\theta$.

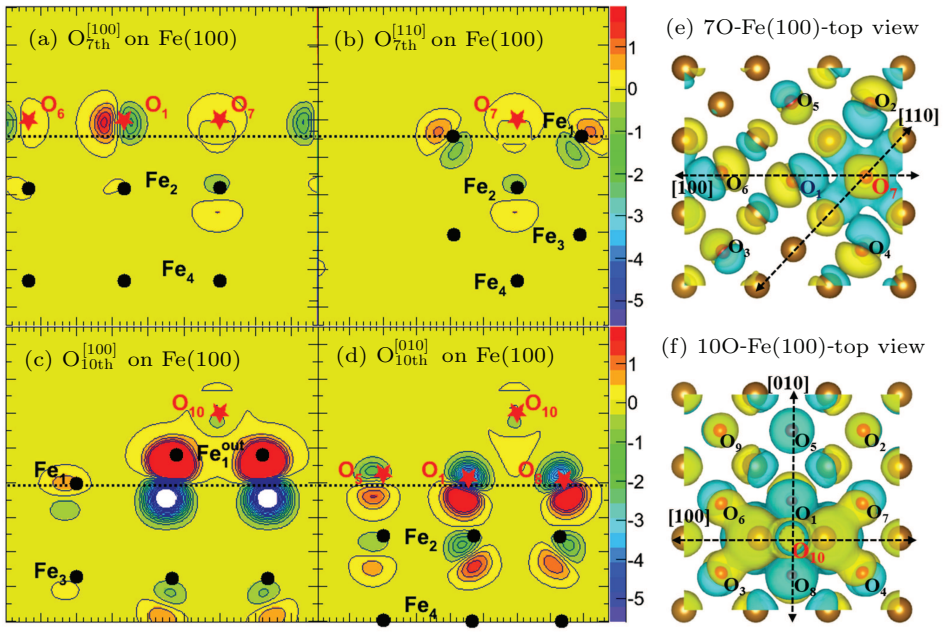



**Fig. 6.** Two-dimensional side view of charge density difference around the 7th O atom adsorbed on the Fe (100) surface by cutting off the model along [100] (a) and [110] (b), and around the 10th O adsorbed on the Fe(100) surface by cutting off the model along [100] (c) and [010] (d). Three-dimensional top view of charge density difference around the 7th O atom (e) and 10th O atom (f) on the Fe(100) surface. In (a)–(d), red stars and black dots represent the adsorbed O atoms and Fe atoms on/in the surface/near-surface region. $O_1$, $O_5$, $O_6$, $O_7$, ... are O atoms with the adsorption sequence and the $Fe_1$, $Fe_2$, $Fe_3$, ... indicate Fe atoms at different layer. The accumulation or depletion of charges are demonstrated by the color scale in (a)–(d). Yellow and blue colors in (e) and (f) refer to electron accumulation and depletion zones, respectively. Brown and red balls are labeled as Fe and O atoms, respectively. The iso-surface of charge density is 0.008 $e$/Bohr$^3$.

### 3.3. The effects of oxygen coverage on oxidation corrosion

As we know, the higher oxygen concentration in the environment, the faster oxidation of Fe-based structure materials. The effects of oxygen coverage on the solution of O atoms in the near-surface region are energetically explored and discussed in this section. The solution energy of one O atom at the near-surface region and bulk region in the model is calculated based on the most stable configurations of O atoms with different coverage. As shown in Fig. 7, the solution energy $E_{\rm sol}^{\rm 1O}$ of one O atom near the surfaces increases quickly, as it moves from the surface to the near-surface region, and converges to constant in the bulk region. This indicates that O atoms prefer surfaces to bulk. When the coverage of O atoms on the Fe(100)/Fe(110) surface is below 0.67/0.22, the O atom in the near-surface region (2nd and 3nd layer) is unstable and spontaneously moves to the surface after relaxation. However, when the coverage increases, the adsorption energies of O atoms increase, the segregation energies of O atoms (the adsorption energy of an O atom on the surface subtracting solution energy of an O atom in bulk) increase as shown in Fig. 7. Therefore, O atoms can stably stay at the octahedron positions in the near-surface region at high coverage, so that the high coverage of O atoms on the surfaces can promote the solution of O atoms in the near-surface region and oxidation corrosion. Moreover, the solution energies of O atoms in the near-Fe(110) surface region are generally higher than those in the near-Fe(100) surface region, indicating that O atoms dissolve in the near-Fe(110) region more hardly than in the near-Fe(100) region.

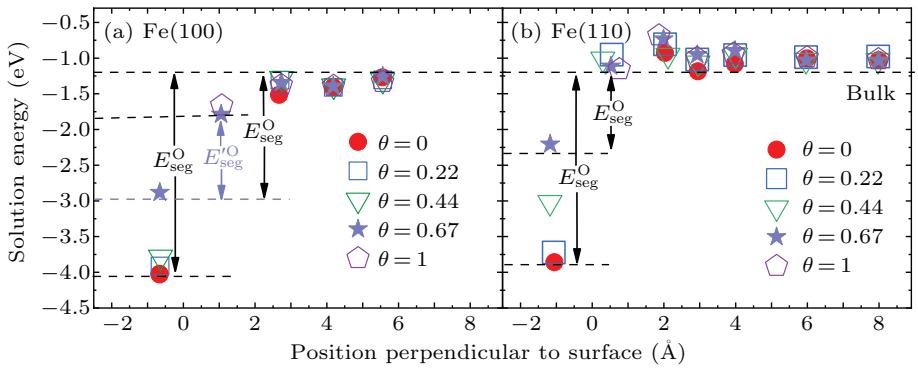



**Fig. 7.** Solution energies of interstitial O atoms in near-surface with different surface coverage of O atoms on Fe (100) (a) and Fe (110) (b), respectively. The black horizontal dash line indicates the solution energy (−1.20 eV[15,16,22]) of an interstitial O atom at octahedron position in bulk.

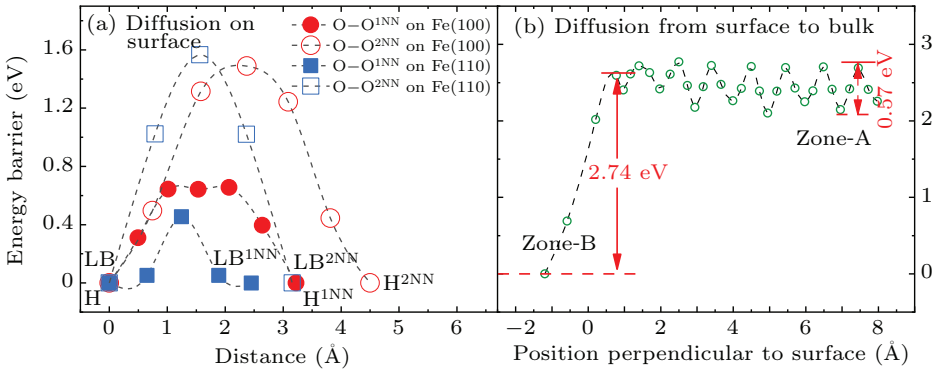



**Fig. 8.** (a) The energy barrier of one O atom migrating from one "H" to its first neighbor "H" and second neighbor "H" on Fe(100) (a) and from one "LB" to its first neighbor "LB" and second neighbor "LB" on Fe (110), respectively. (b) The energy diagram of O atoms migrating from the Fe(110) surface with oxygen coverage of 1/4 to the bulk-like region.

The dynamic properties of O atoms on the Fe surfaces are investigated through the energy barriers of O atoms diffusing on the surfaces. Figure 8(a) shows the energy barriers of O atoms migrating on Fe(100) and Fe(110) surfaces in different paths, respectively. An O atom has to overcome an energy barrier of 0.65 eV and 1.48 eV for migrating in the paths of H–$H^{1NN}$ and H–$H^{2NN}$ on Fe(100) surface, respectively. Meanwhile, it overcomes 0.45 eV and 1.56 eV for migrating in paths of LB–$LB^{1NN}$ and LB–$LB^{2NN}$ on Fe(110) surface, respectively. This indicates that O atoms prefer to move from one most stable to their first neighbor's most stable positions. Meanwhile, the energy barrier of O atoms diffusing on the Fe(110) surface is lower than that on Fe(100) surface, indicating that the diffusion of O atoms on the Fe(110) surface is easier than that on Fe(100) surface.

Besides, the dynamic behavior of O atoms from surface to bulk is further explored and compared with that on the surfaces. Here, the Fe(110) with oxygen coverage of 1/4 is taken as an example, since O atoms can stay at the near-surface region. As shown in Fig. 8(b), one of O atom needs to overcome 2.74 eV to migrate into the near-surface region, while 0.57 eV to diffusion in bulk region, showing good agreement with previous results (0.53 eV[16,20]). The energy barriers of O atoms migrating from the surface to the bulk region are significantly higher than those on the surfaces, therefore, O atoms prefer to diffuse on the surfaces compared to the bulk region. Therefore, when bcc-Fe-based structure materials are in contact with the oxygen contained environment, O atoms would adsorb and then diffuse on the surfaces with low oxygen coverage, and finally go through the near-surface region with the repulsion of O atoms adsorbed on the surfaces with high coverage.

### 3.4. The effects of irradiation defects on oxidation corrosion

The effects of vacancies on oxidation corrosion are investigated by the binding energy $E_{bin}^{v+O}$ between vacancy and O atoms. Firstly, the energetics characters of vacancy are investigated by the vacancy formation energies $E_f^v$, defined as the total energies of the surface slab with one vacancy and one Fe atom in bulk subtracting the energy of the surface slab without any vacancy.[57] The vacancy formation energies on Fe(100) and (110) surfaces in Fig. 9 show a critical increase trend as the distance to the surface increases and converges to constant at bulk region. This is consistent with previous theoretical studies (2.15 eV[16,20,23]), and again indicates that our model is reasonable to mimic the vacancy behavior on the surfaces and in the near-surface region.

Then, the solution energies of O atoms near vacancies in near-surface and bulk regions are calculated according to Eq. (3) for investigating the effects of vacancies on the solution of O atoms. As shown in Fig. 10(a), the solution energies of O atoms near vacancies increase with the increasing depth of oxygen atoms from the surface. The increasing trend is the same as that in the surface model without any vacancies. However, the adsorption energies of O atoms are almost not changed as O atoms are adsorbed on the surfaces, but the solution energies of O atoms are much reduced by vacancies in near-surface and bulk regions. This leads to an obvious increase in the segregation energies of O atoms due to the vacancies (e.g., from −2.76 eV to −1.28 eV). Therefore, O atoms can be easily bound by vacancies, which reversely affect the solution of O atoms in near-surface and bulk-region.

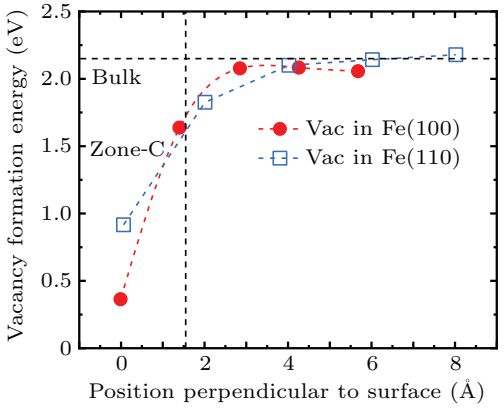



**Fig. 9.** Vacancy formation energies ($E_f^v$) are functions of the distance from the surface.

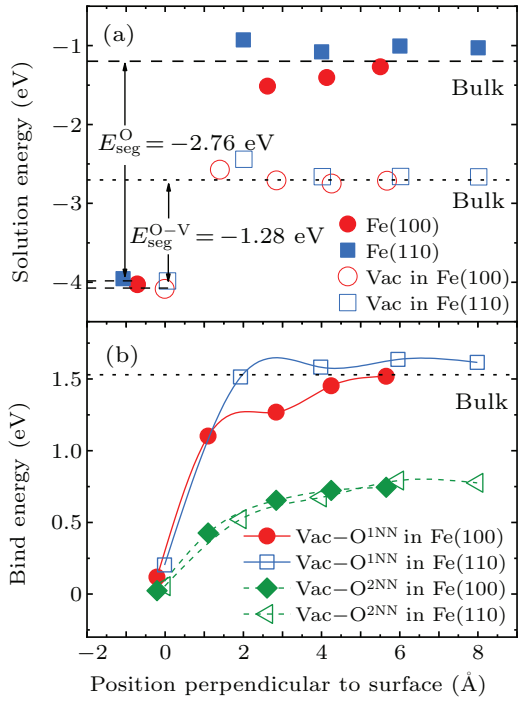



**Fig. 10.** (a) Solution energies of an O atom with or without vacancy at different distances to the surfaces with different coverage. The black horizontal dash lines indicate the solution energies of an O atom located on OCT in bulk with and without a vacancy nearby. $E_{seg}^{O}$ indicate the segregation energies of O atoms on the Fe(100) and (110) surfaces with and without vacancies. (b) Binding energies ($E_{bin}^{v+O}$) of the vacancy with oxygen as functions of their distance to the (100) and (110) surfaces. The green solid diamonds and open triangles in (b) indicate O atoms are the second nearest neighbors (2NN) to the vacancies. The black horizontal dash line indicates the binding energy of an O atom and vacancy in bulk.

Besides, the binding energy $E_{bin}^{v+O}$ of one vacancy and an O atom is obtained according to Eq. (5) and shown in Fig. 10(b). The binding energies $E_{bin}^{v+O}$ between one vacancy and its first nearest neighbor ($E_{bin}^{v+O^{1NN}}$) or second nearest neighbor O atom ($E_{bin}^{v+O^{2NN}}$) show a general increase trend from surface to near-surface region, and the binding energies $E_{bin}^{v+O^{1NN}}$ converge to 1.5 eV in the bulk region. Both $E_{bin}^{v+O^{1NN}}$ and $E_{bin}^{v+O^{2NN}}$ on surfaces are near zero, and less than these in the bulk region. The interaction between one vacancy and its first nearest and second neighbor O atom is very small, while is strong in the bulk region. Meanwhile, the $E_{bin}^{v+O^{1NN}}$ is generally greater than $E_{bin}^{v+O^{2NN}}$, indicating that the effect of a vacancy on an O atom at its first nearest neighbor is greater than at its second nearest neighbor, especially in the near-surface and bulk region.

The effects of vacancies on the dynamic behavior of O atoms are studied by the energy barriers of O atoms around a vacancy diffusing from the surface towards the near-surface region. The Fe(110) with coverages of 1/4 and 1/2 is again taken as examples for comparing with the diffusion of an O atom in a defect-free surface system shown in Fig. 8. As shown in Fig. 11(a), an O atom diffuses from a first nearest neighbor of the vacancy on the surfaces to another first nearest neighbor position in the near-surface region. The energy barrier of an O atom around a vacancy on the Fe(110) surface with coverage of 1/4 is 1.87 eV in Fig. 11(b), which is much less than 2.74 eV in the defect-free system. The energy barrier of an O atom around a vacancy on the Fe(110) is reduced to be 1.18 eV, as the coverage of O atoms increases from 1/4 to 1/2. These results indicate that both vacancies and oxygen concentration could accelerate the diffusion of O atoms into the near-surface region, and further lead to quick oxidation in experiments.

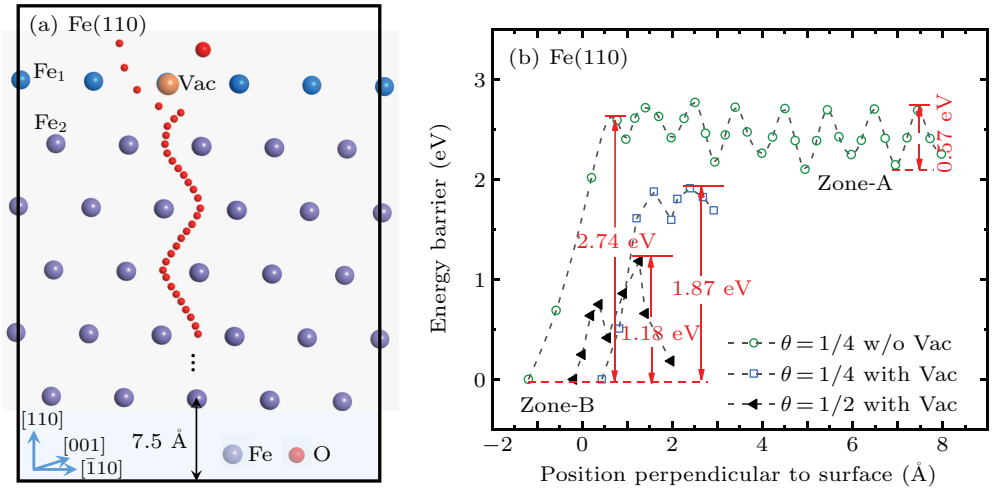



**Fig. 11.** (a) The migration path diagram of O atoms with and without (w/o) a vacancy migrating from the Fe(110) surface to the subsurface when the coverage increases from 1/4 to 1/2, and (b) the corresponding migration energy diagram.

### 3.5. Discussion

As we know, oxidation of bcc-Fe-based steels would be accelerated under either high oxygen concentration or irradiation. The picture of the oxidation of bcc-Fe surfaces at the initial stage has been sketched in Fig. 12 based on the above studies on the adsorption/solution and migration properties of O atoms on/under the surfaces with different coverage of O

atoms and vacancies. In a low oxygen concentration environment, O atoms adsorb on the surfaces with low coverage, and probably diffuse on the surfaces. With irradiation-induced vacancies, they would migrate into the bulk region. In a high oxygen concentration environment, O atoms adsorb on Fe surfaces with high coverage, and then further diffuse into the bulk region with the repulsion from the continuously approaching O atoms from the environment. Meanwhile, Fe atoms on the surfaces are pulled out, leaving more space for O atoms.

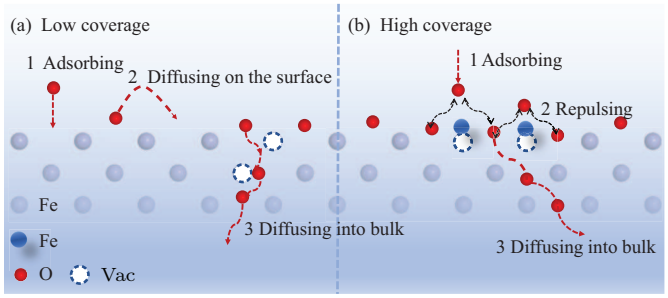



**Fig. 12.** The oxidation mechanism of Fe surfaces with low oxygen coverage (a) and high oxygen coverage (b). 1 and 3 indicate the adsorbing of O atoms on the surfaces and the diffusion of O atoms from the surface into bulk. 2 indicates the diffusing processes of O atoms on the surfaces with low oxygen coverage and repulsing processes between O atoms on the surfaces with high oxygen coverage. The grey and red balls indicate the Fe atoms in lattice and O atoms, while blue balls and blue dashed circles represent Fe atoms pulled out and vacancies, respectively.

To intuitively describe the effects of oxygen concentration and irradiation on oxidation, we try to estimate an equilibrium oxygen density in near-surface and bulk regions. Ignoring the interactions between O atoms at the same atomic layers in the near-surface and bulk region, the relationship of concentration of oxygen on surfaces and in bulk can be described by the McLean's equation[58–60]

$$\frac{C_{\rm surf}}{1-C_{\rm surf}}=\frac{C_{\rm bulk}}{1-C_{\rm bulk}}\,{\rm e}^{\frac{-E^{\rm O}_{\rm seg}}{kT}}, \tag{6}$$

where $C_{\rm surf}$ and $C_{\rm bulk}$ represent the concentration of oxygen on the surfaces and in the bulk, $E^{\rm O}_{\rm seg}$ is the segregation energy labelled in Figs. 7 and 10, $T$ is the environment temperature and $k$ is the Boltzmann constant. Inversely, as the concentration of oxygen in the environment is known, the concentration of oxygen in the near-surface and bulk region can be estimated by

$$C_{\rm bulk}=\frac{C_{\rm surf}}{C_{\rm surf}+(1-C_{\rm surf})\,{\rm e}^{\frac{-E'^{\rm O}_{\rm seg}}{kT}}}, \tag{7}$$

where $E'^{\rm O}_{\rm seg}$ indicates that the energy needed for an O atom segregating from near-surface or bulk region to the surface with a certain coverage, as labeled in Fig. 7.

The effect of oxygen concentration on oxidation is firstly investigated by the density of O atoms at the atomic layers in the near-surface and bulk region with different coverage of O atoms on the surfaces. The density of oxygen on the surfaces is taken as a constant value and calculated by the number of O atoms divided by the area of the surface. Taken the Fe(100) surface as examples, the oxygen coverages of 1/9, 6/9 and 1 correspond to the oxygen densities of $1.39\times10^{-2}$ Å$^{-2}$, $8.32\times10^{-2}$ Å$^{-2}$ and $1.25\times10^{-1}$ Å$^{-2}$, respectively. Given the experimental temperature of 800 K, the $E'^{\rm O}_{\rm seg}$ values of O atoms at the near-surface and bulk region can be obtained according to the solution energies of O atoms as shown in Fig. 7. Based on the $E'^{\rm O}_{\rm seg}$ values, the density of oxygen on the second layer, third layer, ... and bulk can be evaluated according to Eq. (7), and shown in Fig. 13. It can be seen from Fig. 13(a), the densities of O atoms generally increase with the increase in the segregation energy. The higher density of O atoms on the surface, the higher densities of O atoms corresponding to the greater segregation energies of O atoms in the near-surface and bulk. Besides, the distribution character of O atoms in the direction of perpendicular to the surface is explored and shown in Fig. 13(b). In a low oxygen concentration environment ($\theta<0.67$), the density of O atoms decreases from surface to bulk region, and the oxygen concentration gradient is obvious in the region. However, the density of O atoms varies little from surface to the bulk region in high oxygen concentration environment ($\theta=1$) and is several orders of magnitude greater than that in a low oxygen concentration environment. This is mainly induced by the sudden increase in the adsorption energy of an O atom on the surface with $\theta$ of 1, therefore O atoms prefer to stay in the bulk region. As the density of O atoms increases, the interaction between the adsorbing O atom and the pre-covered O atoms increases, which also has been discussed by the charge density difference around O atoms on the surfaces with high coverage as shown in Fig. 6.

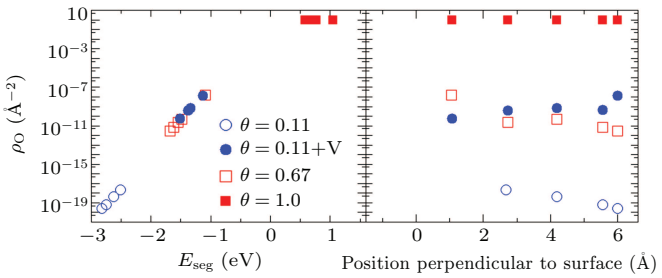



**Fig. 13.** The concentrations of oxygen as function of the energy of an oxygen segregating from near surface or bulk region to the surface (a), and the position of an oxygen perpendicular to the Fe(100) surface (b). The blue open circles, red open squares and red solid squares represent the densities of oxygen at different positions relative to the surface with oxygen coverage of 0.11, 0.67 and 1.0, respectively. The blue solid circles are the densities of oxygen in near-surface and bulk region with low coverage of oxygen and vacancies.

In addition, the effect of irradiation on oxidation is explored by the density of O atoms at the atomic layers with vacancies nearby in the near-surface and bulk region. Besides

the effects of O atoms on the surfaces, other interactions between O atoms or vacancies nearby are not considered in the model. With the same low coverage of O atoms on the surface (1/9), vacancies decrease the solution energies of O atoms in the near-surface and bulk region as shown in Fig. 10(a), and obviously improve the segregation energies. Therefore, the densities of O atoms in the near-surface and bulk region would be significantly promoted in several orders of magnitude by the irradiated vacancies. Meanwhile, the density of O atoms under the surfaces does not depend on the depth of O atoms from the surface. This is due to the very simple hypothesis here, which vacancies distribute the same at the surface and bulk, and interactions between vacancies are ignored. The effects of irradiation on the distribution of O atoms in the near-surface region will be further studied in the next work at a large scale with these parameters.

## 4. Conclusions

Based on first-principles calculations, the oxidation mechanism of bcc-Fe surfaces at the initial stage is explored by systematically investigating the adsorption/solution properties and diffusion behavior of oxygen atoms on/under iron surfaces. The adsorption energies show that surfaces have a strong attraction to oxygen atoms, and the attraction strength depends on the local structure and oxygen coverage. The solution energies of O atoms are closely related to the coverage of oxygen atoms adsorbed on the surfaces and irradiated vacancies in near-surface and bulk regions. With the increase in oxygen coverage and vacancies, oxygen atoms gradually dissolve in the near-surface region. Dynamic results indicate that the oxygen atoms prefer to diffuse on the surfaces than into the near-surface region, and the diffusion process is promoted by the coverage of oxygen atoms on the surface and vacancies. Moreover, the effects of oxygen concentration and irradiation on oxidation are roughly estimated by the McLean's model with a simple hypothesis. This paper reveals the microscopic mechanism of oxidation corrosion of O atoms on Fe surfaces, provides parameters for the further investigation of oxidation corrosion under nuclear energy irradiation environment.

## Acknowledgements

Project supported by the National Key Research and Development Program of China (Grant Nos. 2017YFE0302400 and 2017YFA0402803), the National Nature Science Foundation of China (Grant Nos. 11735015, 52071314, 51871207, U1832206, 12075274, U1967211, 52171084), and Hefei Advanced Computing Center.

## References

[1] Martinelli L, Balbaud-Célérier F, Terlain A, Bosonnet S, Picard G and Santarini G 2008 *Corros. Sci* **50** 2537
[2] Fazio C 2015 *Handbook on lead-bismuth eutectic alloy and lead properties, materials compatibility, thermal-hydraulics and technologies* (Paris: Organization for Economic Cooperation and Development/Nuclear Energy Association) pp. 431–478
[3] Wagner C 1969 *Corros. Sci* **9** 91
[4] Yeliseyeva O, Tsisar V and Benamati G 2008 *Corros. Sci* **50** 1672
[5] Zhang J and Li N 2008 *J. Nucl. Mater.* **373** 351
[6] Schroer C, Tsisar V, Durand A, Wedemeyer O, Skrypnik A and Konys J 2019 *J. Nucl. Eng. Radiat. Sci.* **5** 011006
[7] Gorynin I V, Karzov G P, Markov V G and Yakovlev V A 1999 *Met. Sci. Heat Treat.* **41** 9
[8] Barbier F and Rusanov A 2001 *J. Nucl. Mater.* **296** 231
[9] Frazer D, Qvist S, Parker S, Krumwiede D L, Caro M, Tesmer J, Maloy S A, Wang Y Q and Hosemann P 2016 *J. Nucl. Mater.* **479** 382
[10] Yao C, Wang Z, Zhang H, Chang H, Sheng Y, Shen T, Zhu Y, Pang L, Cui M, Wei K, Sun J, Peng T, Liu C and Ma Z 2019 *J. Nucl. Mater.* **523** 260
[11] Xing H, Hu P, Li S, Zuo Y, Han J, Hua X, Wang K, Yang F, Feng P and Chang T 2021 *J. Mater. Sci. Technol.* **62** 180
[12] Błoński P, Kiejna A and Hafner J 2005 *Surf. Sci.* **590** 88
[13] Błoński P, Kiejna A and Hafner J 2007 *J. Phys.: Condens. Matter* **19** 096011
[14] Nishihara K, Nomitsu T, Nakagawa T and Mizuno S 2019 *Surf. Sci.* **685** 34
[15] Barouh C, Schuler T, Fu C C and Nastar M 2014 *Phys. Rev. B* **90** 054112
[16] Fu C L, Krcmar M, Painter G S and Chen X Q 2007 *Phys. Rev. Lett* **99** 225502
[17] Barouh C, Schuler T, Fu C C and Jourdan T 2015 *Phys. Rev. B* **92** 104102
[18] Yuan X, Song C, Kong X, Xu Y, Fang Q F and Liu C S 2013 *Physica B* **425** 42
[19] Ropo M, Punkkinen M, Kuopanportti P, Yasir M, Granroth S, Kuronen A and Kokko K 2021 *Sci. Rep.* **11** 6046
[20] Shang S L, Fang H Z, Wang J, Guo C P, Wang Y, Jablonski P D, Du Y and Liu Z K 2014 *Corros. Sci* **83** 94
[21] Wang X, Posselt M and Faßbender J 2018 *Phys. Rev. B* **98** 064103
[22] Liu Z J, Zhang Y G, Li X Y, Xu Y C, Wu X B, Liu C S, Kong X S, Yao C F and Wang Z G 2021 *RSC Advances* **11** 8643
[23] Wang X, Faßbender J and Posselt M 2020 *Phys. Rev. B* **101** 174107
[24] Byggmastar J, Nagel M, Albe K, Henriksson K O E and Nordlund K 2019 *J. Phys.: Condes. Matter* **31** 215401
[25] Kresse G and Hafner J 1993 *Phys. Rev. B* **47** 558
[26] Kresse F G 1996 *Phys. Rev. B* **54** 11169
[27] Perdew J P and Ernzerhof M 1998 *Phys. Rev. Lett.* **80** 891
[28] Kresse J G 1999 *Phys. Rev. B* **59** 1758
[29] Blochl P E 1994 *Phys. Rev. B* **50** 17953
[30] Han J H and Oda T 2017 *Phys. Chem. Chem. Phys.* **19** 9945
[31] Nandi P K, Valsakumar M C, Chandra S, Sahu H K and Sundar C S 2010 *J. Phys.: Condes. Matter* **22** 345501
[32] Levesque M, Gupta M and Gupta R P 2012 *Phys. Rev. B* **85** 064111
[33] Zhang Y G, You Y W, Li D D, Xu Y C, Liu C S, Pan B C and Wang Z G 2015 *Phys. Chem. Chem. Phys.* **17** 12292
[34] Monkhorst H J and Pack J D 1976 *Phys. Rev. B* **13** 5188
[35] Chen L, Li Y F, Zheng Q L, Liu Q K, Gao Y M, Li B and Zhou C M 2019 *Acta Phys. Sin.* **68** 053101 (in Chinese)
[36] Shu Y, Zhang Y and Zhang J M 2012 *Acta Phys. Sin.* **61** 016108 (in Chinese)
[37] Liu K, Wang F H and Shang J X 2017 *Acta Phys. Sin.* **66** 216801 (in Chinese)
[38] Ossowski T and Kiejna A 2015 *Surf. Sci.* **637** 35
[39] Shimada T, Ishii Y and Kitamura T 2010 *Phys. Rev. B* **81** 134420
[40] Ma J X, Jia Y, Liang E J, Wang X C, Wang F and Hu X 2003 *Acta Phys. Sin.* **52** 3155 (in Chinese)
[41] Song C, Li D D, Xu Y C, Pan B C, Liu C S and Wang Z G 2014 *Chin. Phys. B* **23** 056801
[42] Xu Y C, Song C, Zhang Y G, Liu C S, Pan B C and Wang Z G 2014 *Phys. Chem. Chem. Phys.* **16** 16837
[43] Zhang F C, Liu Y and Zhang W B 2015 *Chin. Phys. Lett.* **32** 057302

[44] Chen Y H, Cao Y J and Ren B X 2010 *Acta Phys. Sin.* **59** 8015 (in Chinese)
[45] Wu X X, Wang Q E, Wang F H and Zhou Y S 2010 *Acta Phys. Sin.* **59** 7278 (in Chinese)
[46] Fang C H, Shang J X and Liu Z H 2012 *Acta Phys. Sin.* **61** 047101 (in Chinese)
[47] Xiong H H, Liu Z, Zhang H H, Zhou Y and Yu Y 2017 *Acta Phys. Sin.* **66** 168101 (in Chinese)
[48] Wei Y W and Yang Z X 2008 *Acta Phys. Sin.* **57** 7139 (in Chinese)
[49] Yang Y, Liu F C and Kawazoe Y 2018 *Chin. Phys. B* **27** 106801
[50] Liu C G, Yu L M, Liu Y C, Ma Z Q, Li H J, Li C and Liu C X 2020 *AIP Adv.* **10** 025309
[51] Błoński P and Kiejna A 2007 *Surf. Sci.* **601** 123
[52] Tan X, Zhou J and Peng Y 2012 *Appl. Surf. Sci.* **258** 8484
[53] Spencer J S, Snook I K and Yarovsky I 2002 *Surf. Sci.* **513** 389
[54] Błoński P, Kiejna A and Hafner J 2008 *Phys. Rev. B* **77** 155424
[55] Bader R F W 1990 *Atoms in Molecules: A Quantum Theory*, 1nd Edn. (New York: Oxford University Press) pp. 78–85
[56] Henkelman G, Arnaldsson A and Jónsson H 2006 *Comput. Mater. Sci.* **36** 354
[57] Sun M and Wang C Y 2016 *Chin. Phys. B* **25** 067104
[58] Stefano D D, Nazarov R, Hickel T, Neugebauer J, Mrovec M and Elsasser C 2016 *Phys. Rev. B* **93** 184108
[59] McLean D 1957 *Grain Boundaries in Metals* (Oxford: Clarendon Press) pp. 116–121
[60] Lejcek P 2010 *Grain Boundary Segregation in Metals* (Berlin: Springer) pp. 51–81